JACS
JOURNAL OF THE AMERICAN CHEMICAL SOCIETY
Communication
pubs.acs.org/JACS

First-Principles Study of Ion Diffusion in Perovskite Solar Cell Sensitizers

Jun Haruyama,*[,†] Keitaro Sodeyama,[‡,§] Liyuan Han,[∥,⊥] and Yoshitaka Tateyama*[,†,‡,§,⊥]

[†]Global Research Center for Environmental and Energy Nanoscience (GREEN) and [‡]International Center for Materials Nanoarchitectonics (MANA), National Institute for Materials Science, 1-1 Namiki, Tsukuba, Ibaraki 305-0044, Japan
[§]Elements Strategy Initiative for Catalysts & Batteries, Kyoto University, Nishikyo-ku, Kyoto 615-8245, Japan
[∥]Photovoltaic Materials Unit, National Institute for Materials Science, 1-2-1 Sengen, Tsukuba, Ibaraki 305-0047, Japan
[⊥]PRESTO and CREST, Japan Science and Technology Agency, 4-1-8 Honcho, Kawaguchi, Saitama 333-0012, Japan

Supporting Information

ABSTRACT: Hysteresis in current−voltage curves has been an important issue for conversion efficiency evaluation and development of perovskite solar cells (PSCs). In this study, we explored the ion diffusion effects in tetragonal $CH_3NH_3PbI_3$ ($MAPbI_3$) and trigonal $(NH_2)_2CHPbI_3$ ($FAPbI_3$) by first-principles calculations. The calculated activation energies of the anionic and cationic vacancy migrations clearly show that I^- anions in both $MAPbI_3$ and $FAPbI_3$ can easily diffuse with low barriers of ca. 0.45 eV, comparable to that observed in ion-conducting materials. More interestingly, typical MA^+ cations and larger FA^+ cations both have rather low barriers as well, indicating that the cation molecules can migrate in the perovskite sensitizers when a bias voltage is applied. These results can explain the ion displacement scenario recently proposed by experiments. With the dilute diffusion theory, we discuss that smaller vacancy concentrations (higher crystallinity) and replacement of MA^+ with larger cation molecules will be essential for suppressing hysteresis as well as preventing aging behavior of PSC photosensitizers.

Perovskite solar cells (PSCs) based on organometal halide materials have attracted considerable attention because the power conversion efficiencies (PCEs) have increased from 3.8% to 20.1% in the last 5 years.[1−11] This rapid increase is attributed to the remarkable properties of lead halide perovskite for solar cell applications: high optical absorption coefficients,[12] long diffusion lengths of both electrons and holes,[13−15] and high mobility of charge carriers.[16] These characteristics are theoretically elucidated by the electronic structures,[17] including a suitable band gap, strong transition dipole moment,[18] low effective masses of the carriers,[19−21] and shallow defect levels.[22−24] Especially, the absence of additional midgap states leads to few carrier traps and nonradiative recombination centers even in the presence of defects, which results in the long diffusion length.[15,25]

Despite these outstanding properties of perovskite sensitizers, one concern has recently arisen: anomalous hysteresis in the PSC's current−voltage (J−V) curves, as reported by Dualeh and Snaith.[26,27] The dependence of J−V curves on the voltage scan direction and speed makes it more difficult to evaluate the PCE. Understanding and resolving the hysteretic behavior is thus essential for the improvement of PCE. Some experiments indicate that crystal size and low-frequency response are related to the hysteresis,[28−30] whereas the origin remains unclear. Many researchers have proposed various types of explanations such as ferroelectricity[31] or structural changes.[32] In particular, Tress et al. recently suggested ion displacement in the perovskite sensitizer for the origin.[33] They showed that the rate-dependent hysteresis seen in J−V scans is related to a slow field-induced process that tends to cancel the electric field in the device at each applied bias voltage. Their mechanism, built-up potential induced by ion displacement to screen the applied bias and decrease of the open-circuit voltage or the steady-state photocurrent, well explains the observed J−V curve behaviors. They also pointed out aging of PSCs due to the presence of mobile ions. Thus, understanding ion behavior in the perovskite materials is essential not only for suppressing hysteresis but also for preventing aging of PSCs.

In this study, we focused on ion migration behavior in perovskite sensitizers to elucidate possible mechanisms of the hysteresis. We carried out first-principles density functional theory (DFT) calculations of the activation energies ΔE_a of vacancy/impurity migrations, which seem most dominant ion diffusion processes, in typical tetragonal $CH_3NH_3PbI_3$ ($MAPbI_3$) and trigonal $(NH_2)_2CHPbI_3$ ($FAPbI_3$) with larger cations.[9] Here we considered vacancy migrations of V_I/V_I^+, V_{MA}/V_{MA}^-, and V_{FA}/V_{FA}^-, which we expected to be fast-diffusing species because they represent vacancies of low-valence ions. We excluded Pb^{2+} migration because high-charged ions are likely to require high activation energies. In addition, taking into account the $MAPbI_{3-x}Cl_x$ phase, we examined migrations of Cl impurity with vacancy (I_{Cl}/I_{Cl}^+). Comparing with other ion-conducting materials, we demonstrate that not only anions but also cation molecules can diffuse in the perovskite sensitizers. The present results enable us to discuss suppression of both hysteresis and aging phenomena.

DFT calculations were carried out within the plane wave basis, pseudopotential, and spin-unpolarized framework as implemented in the QUANTUM-ESPRESSO package.[34] The vdW-DF2-B86R functional including van der Waals interaction[35] were

Received: April 7, 2015
Published: August 10, 2015

DOI: 10.1021/jacs.5b03615
J. Am. Chem. Soc. 2015, 137, 10048−10051

used. The optimized parameters of the perfect crystals are in good agreement with the experimental values and previous DFT calculations.[36−39] Detailed computational conditions are described in the Supporting Information (SI).

Figure 1 shows four paths of vacancy migration calculated in this study. The arrows P1 and P2 represent V_I migration in the

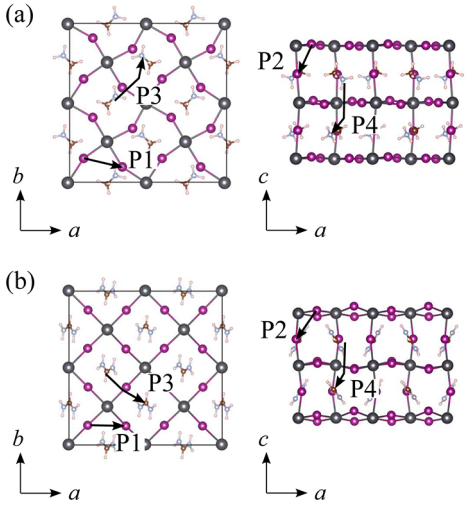

Figure 1. Vacancy migration paths of (a) $MAPbI_3$ and (b) $FAPbI_3$. Arrows P1, P2 and P3, P4 represent V_I and V_{MA} (or V_{FA}) paths, respectively. The H, C, N, I, and Pb atoms are depicted as white, brown, light blue, purple, and black spheres, respectively.

⟨100⟩ and ⟨111⟩ directions, respectively, while V_{MA} (or V_{FA}) migration along the ⟨110⟩ and ⟨001⟩ directions are indicated by arrows P3 and P4, respectively. These indices are based on the tetragonal cell. Since the four paths represent elemental processes of the vacancy migration, an overall ion-diffusion mechanism can be understood by combining these migrations. Interstitial-defect migrations are also a possible microscopic process and should be investigated in future studies; here we focused on vacancy-mediated diffusion as a first step because lower barriers are expected for this type of diffusion.

Figure 2 illustrates the energy profiles along the vacancy migration paths of P1 and P3. The configuration of the start point ($x = 0$) is defined such that the migrating vacancy is placed at the end of the arrow as illustrated in Figure 1. In the same manner, the end point ($x = 1$) is defined as the vacancy located at the start of the arrow. In Figure 2a, the higher energy at the start point than the end is attributed to the inequivalency induced by the surrounding MA orientations (see Figure S3 and discussions in SI). We take the larger activation energy from the end point throughout this study. The V_I^+ curve exhibits almost the same energy profile as that of V_I because the excess hole finally goes to a delocalized state owing to the buried transition level between V_I/V_I^+ in the conduction band.[17,23] These results show that the activation barrier of V_I migration in the ⟨100⟩ direction is ca. 0.3 eV. This can be understood in terms of a covalent-bond aspect as well. Since the valence band of $MAPbI_3$ has strong Pb-s and I-p antibonding character,[17,23] Pb−I bonds are weak enough for I^- migration. We emphasize that a barrier of 0.3 eV is very small and comparable to that of fast ion-conducting materials (e.g., Li-ion conductors). These results clearly indicate intense V_I diffusion in the $MAPbI_3$ crystal.

On the other hand, the energy along the P3 path, depicted in Figure 2b, indicates a slightly higher activation barrier. Yet, the

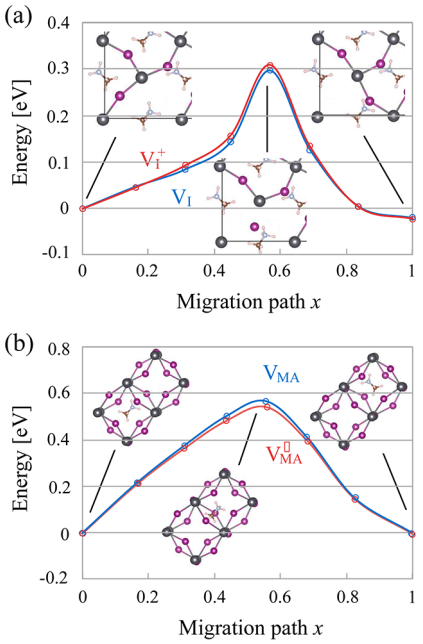

Figure 2. Energy profiles along the migration paths of (a) P1 and (b) P3 in $MAPbI_3$. The path of V_I (V_{MA}) corresponds to the neutral system, whereas that of V_I^+ (V_{MA}^-) reflects a system in which one electron is removed from (or added to) the calculation supercell. The insets show the structures of the NEB images at the initial, transition, and final states.

calculated barrier of V_{MA} (0.57 eV) suggests that MA cations can diffuse easily in contrast to the expectation based on the molecular size. It is likely that ionic interaction between MA^+ cation and the PbI_3^- lattice is rather weak because of their low ionic charges, and MA^+ can easily rotate. Consequently, the activation barrier of V_{MA} migration is small enough. The present results provide significant insight by showing that both anion and cation diffusions can concurrently take place while maintaining charge neutrality. This is likely to be the detailed atomistic mechanism of ion displacement proposed for the rate-dependent hysteresis of the $J-V$ curves. These ion diffusions may inhibit the charge carrier (electron and hole) transport. We also suggest that the cation migration is undesirable for the aging of perovskite sensitizers, because the cations play a role in maintaining the PbI_6 octahedron framework and their diffusions will seriously induce the lattice distortion and contraction, leading to irreversible change of the structure. All the calculated energy profiles and the corresponding configurations of I and MA are depicted in Figures S4 and S5.

The activation barriers of the examined vacancy migrations in $MAPbI_3$ are summarized in Table 1. The values of ΔE_a corresponding to V_I migrations show slight difference between the ⟨100⟩ and ⟨111⟩ directions, while the major activation barrier

Table 1. Calculated Activation Energies ΔE_a of Vacancy and Cl Impurity Migrations in $MAPbI_3$ and $FAPbI_3$ (eV)[a]

path	$MAPbI_3$	$FAPbI_3$	defect	direction
P1	0.32/0.33	0.55/0.50	V_I/V_I^+	⟨100⟩
P2	0.44/0.45	0.48/0.42		⟨111⟩
P3	0.57/0.55	0.61/0.57	V_{MA}/V_{MA}^- or V_{FA}/V_{FA}^-	⟨110⟩
P4	0.89/0.89	0.61/0.59		⟨001⟩
P1	0.32/0.32	−/−	I_{Cl}/I_{Cl}^+	⟨100⟩

[a]The corresponding diffusion directions are also listed.

DOI: 10.1021/jacs.5b03615
J. Am. Chem. Soc. 2015, 137, 10048−10051

in $MAPbI_3$ is 0.44 eV. In contrast, the ΔE_a values of V_{MA} migrations largely depend on the diffusion direction, indicating anisotropic diffusion. The origin of the difference comes from the tetragonal $MAPbI_3$ crystal structure. For example, the configuration of the MA molecule along P3 should pass through $MAPbI_3$ (110) plane constructed by PbI_3 lattice (see Figure S5). Comparison of the (110) and (001) planes shows that the latter shows a large distortion (or constriction). As a result, the ΔE_a increases when MA passes through the (001) plane.

Since inclusion of Cl anions ($MAPbI_{3-x}Cl_x$ phase) was reported to improve the conversion efficiency of PSC,[4] we examined the Cl impurity migrations (I_{Cl}/I_{Cl}^+) as well. The ΔE_a of I_{Cl} migration was found to be 0.32 eV. This value similar to the V_I migration indicates that $MAPbI_3$ lattice is large enough for migration of halogen ions. Therefore, we predict that halide anions can quickly diffuse in $MAPbX_3$ (X = Cl, Br, I) crystals. This insight is consistent with recent experimental observation, rapid halide exchange in $MAPbX_3$.[40] In addition, the Cl diffusion can explain the fact that Cl anions easily escape from $MAPbI_{3-x}Cl_x$ crystal during the fabrication of perovskite sensitizer.[41]

Table 1 also shows the activation energies of the vacancy migrations in $FAPbI_3$ (the energy profiles and configurations of I and FA migrations are shown in Figures S6 and S7). The value of ΔE_a = 0.55 eV corresponding to V_I migrations along the ⟨100⟩ direction in $FAPbI_3$ shows a higher activation barrier than that in $MAPbI_3$. However, ⟨111⟩ migration can occur with a rather low barrier (0.48 eV). This means that the V_I migrations in $FAPbI_3$ are comparable with $MAPbI_3$ because the ⟨111⟩ migrations can result in hopping along various directions including ⟨100⟩. Similarly, the ΔE_a values of V_{FA} migrations show slightly higher values (0.61 eV) than those of the V_{MA} migrations. Though the activation barrier difference between MA and FA is small, we can expect that the cation diffusion depends on the cation size. Namely, the diffusion of larger cation molecules is more suppressed in the perovskite crystals. This result on the ion diffusion is consistent with the experimental observation that PSCs consisting of $FAPbI_3$ exhibit smaller hysteresis than $MAPbI_3$.[9] In contrast to $MAPbI_3$, the anisotropic character of V_{FA} migrations was not obtained here. This is attributed to more symmetric lattice structure of $FAPbI_3$, i.e., the $FAPbI_3$ lattice is closer to a cubic structure than $MAPbI_3$.[39,42]

Here we discuss the origin and suppression of the ion diffusion in $MAPbI_3$. In comparison with ABO_3-type perovskites, some of which are known as oxide-ion conductors,[43] $MAPbI_3$ consists of low-valence ions. As a result, weak ion bonds in $MAPbI_3$ induce intense ion diffusion. In addition, ABO_3 can work as oxide-ion conductor because A and B site cations exhibit no diffusive property. However, MA cations in $MAPbI_3$ crystal easily diffuse and trigger the crystal distortion and contraction. All of these ion diffusion aspects should be avoided to reduce the aging of PSCs.

When the diffusion species are assumed to be at a low concentration, dilute diffusion theory is valid and the diffusivity can be written as

$$D \propto x_D \exp(-\Delta E_a/k_B T)$$

where k_B and T are the Boltzmann constant and a temperature, respectively, and x_D is the concentration of the diffusion-mediating defect.[44] Based on the expression, reducing the defect concentration is a straightforward way for suppressing the diffusions of anions and molecular cations. This suggests that fabrication of high quality crystal is crucial for low $J-V$ hysteresis and antiaging. Recently, some experiments exhibited hysteresis-free devices.[45,46] Especially, Nie's study implies a relationship between hysteresis and defect concentrations.[46] Thus, the large-scale crystalline grains are surely effective for reducing defect concentrations. An alternative way is replacement of the cation molecules with larger ones, because they are expected to show slow migration. Highly stable perovskite devices reported by Mei et al. provide one possible example of the effect of large cations.[47] In contrast, the substitution of the halide component will not prevent I^- diffusion because Br^- and Cl^- can migrate easier. Thus, the suppression of halide ion migration is a problem that remains to be solved.

In conclusion, we investigated anion and cation diffusion effects in tetragonal $MAPbI_3$ and trigonal $FAPbI_3$ by first-principles activation energy calculations of the vacancy and impurity migrations. Our results show that I^- anions in both $MAPbI_3$ and $FAPbI_3$ easily diffuse with low barriers of ca. 0.44 and 0.48 eV, respectively, which is consistent with the experimental observations, and comparable to ion-conducting materials. More importantly, we found that MA^+ and FA^+ cations also have rather low barriers for the migrations (0.57 and 0.61 eV, respectively). These results clearly indicate that the cation molecules in the perovskite materials can migrate when a bias voltage is applied. These accounts for the ion displacement concept proposed for the rate-dependent hysteresis of the $J-V$ curves recently reported.[33] The cation migrations also induce large lattice distortion and contraction, leading to aging of PSC sensitizers. Based on the dilute diffusion theory, we suggest that small defect concentrations in large crystalline grains and replacement of MA^+ with larger cation molecules are promising ways to suppress hysteresis as well as to prevent aging of PSC photosensitizers.

■ ASSOCIATED CONTENT

Supporting Information

The Supporting Information is available free of charge on the ACS Publications website at DOI: 10.1021/jacs.5b03615.

The DFT calculation detail, the optimized structures of the perfect tetragonal $MAPbI_3$ and trigonal $FAPbI_3$, 2 × 2 × 2 tetragonal cells for NEB calculations, local structures in the presence of iodine vacancy, the energy profiles along the migration paths, and the corresponding structures of $MAPbI_3$ and $FAPbI_3$ (PDF)

■ AUTHOR INFORMATION

Corresponding Authors

*HARUYAMA.Jun@nims.go.jp

*TATEYAMA.Yoshitaka@nims.go.jp

Notes

The authors declare no competing financial interest.

■ ACKNOWLEDGMENTS

This work was supported by the Strategic Programs for Innovative Research (SPIRE), MEXT, and the Computational Materials Science Initiative (CMSI), Japan. The calculations were carried out on the supercomputers in NIMS and The University of Tokyo as well as the supercomputers in Kyushu University through the HPCI Systems Research Project (proposal nos. hp140179, hp140110, hp140232, hp150055, and hp150068).

DOI: 10.1021/jacs.5b03615
J. Am. Chem. Soc. 2015, 137, 10048−10051

REFERENCES

(1) Kojima, A.; Teshima, K.; Shirai, Y.; Miyasaka, T. *J. Am. Chem. Soc.* **2009**, *131*, 6050−6051.
(2) Im, J. H.; Lee, C. R.; Lee, J. W.; Park, S. W.; Park, N. G. *Nanoscale* **2011**, *3*, 4088−4093.
(3) Kim, H. S.; Lee, C. R.; Im, J. H.; Lee, K. B.; Moehl, T.; Marchioro, A.; Moon, S. J.; Humphry-Baker, R.; Yum, J. H.; Moser, J. E.; Grätzel, M.; Park, N. G. *Sci. Rep.* **2012**, *2*, 591.
(4) Lee, M. M.; Teuscher, J.; Miyasaka, T.; Murakami, T. N.; Snaith, H. J. *Science* **2012**, *338*, 643−647.
(5) Burschka, J.; Pellet, N.; Moon, S. J.; Humphry-Baker, R.; Gao, P.; Nazeeruddin, M. K.; Grätzel, M. *Nature* **2013**, *499*, 316−319.
(6) Liu, M.; Johnston, M. B.; Snaith, H. J. *Nature* **2013**, *501*, 395−398.
(7) Liu, D.; Kelly, T. L. *Nat. Photonics* **2013**, *8*, 133−138.
(8) Jeon, N. J.; Noh, J. H.; Kim, Y. C.; Yang, W. S.; Ryu, S.; Seok, S. I. *Nat. Mater.* **2014**, *13*, 897−903.
(9) Jeon, N. J.; Noh, J. H.; Yang, W. S.; Kim, Y. C.; Ryu, S.; Seo, J.; Seok, S. I. *Nature* **2015**, *517*, 476−480.
(10) *Best Research-Cell Efficiencies*, National Renewable Energy Laboratory. http://www.nrel.gov/ncpv/images/efficiency_chart.jpg (accessed August 9, 2015).
(11) Wu, Y.; Isram, A.; Yang, X.; Qin, C.; Liu, J.; Zhang, K.; Peng, W.; Han, L. *Energy Environ. Sci.* **2014**, *7*, 2934−2938.
(12) Wolf, S. D.; Holovsky, J.; Moon, S.-J.; Löper, P.; Niesen, B.; Ledinsky, M.; Haug, F.-J.; Yum, J.-H.; Ballif, C. *J. Phys. Chem. Lett.* **2014**, *5*, 1035−1039.
(13) Stranks, S. D.; Eperon, G. E.; Grancini, G.; Menelaou, C.; Alcocer, M. J. P.; Leijtens, T.; Herz, L. M.; Petrozza, A.; Snaith, H. J. *Science* **2013**, *342*, 341−344.
(14) Xing, G.; Mathews, N.; Sun, S.; Lim, S. S.; Lam, Y. M.; Grätzel, M.; Mhaisalkar, S.; Sum, T. C. *Science* **2013**, *342*, 344−347.
(15) Wehrenfennig, C.; Eperon, G. E.; Johnston, M. B.; Snaith, H. J.; Herz, L. M. *Adv. Mater.* **2014**, *26*, 1584−1589.
(16) Ponseca, C. S., Jr.; Savenije, T. J.; Abdellah, M.; Zheng, K.; Yartsev, A.; Pascher, T.; Harlang, T.; Chabera, P.; Pullerits, T.; Stepanov, A.; Wolf, J.-P.; Sundström, V. *J. Am. Chem. Soc.* **2014**, *136*, 5189−5192.
(17) Yin, W.-J.; Yang, J.-H.; Kang, J.; Yan, Y.; Wei, S.-H. *J. Mater. Chem. A* **2015**, *3*, 8926−8942.
(18) Yin, W.-J.; Shi, T.; Yan, Y. *Adv. Mater.* **2014**, *26*, 4653−4658.
(19) Even, J.; Pedesseau, L.; Jancu, J.-M.; Katan, C. *J. Phys. Chem. Lett.* **2013**, *4*, 2999−3005.
(20) Giorgi, G.; Fujisawa, J.-I.; Segawa, H.; Yamashita, K. *J. Phys. Chem. Lett.* **2013**, *4*, 4213−4216.
(21) Umari, P.; Mosconi, E.; De Angelis, F. *Sci. Rep.* **2014**, *4*, 4467.
(22) Kim, J.; Lee, S.-H.; Lee, J. H.; Hong, K.-H. *J. Phys. Chem. Lett.* **2014**, *5*, 1312−1317.
(23) Yin, W.-J.; Shi, T.; Yan, Y. *Appl. Phys. Lett.* **2014**, *104*, 063903.
(24) Haruyama, J.; Sodeyama, K.; Han, L.; Tateyama, Y. *J. Phys. Chem. Lett.* **2014**, *5*, 2903−2909.
(25) Eperon, G. E.; Stranks, S. D.; Menelaou, C.; Johnston, M. B.; Herz, L. M.; Snaith, H. J. *Energy Environ. Sci.* **2014**, *7*, 982−988.
(26) Dualeh, A.; Moehl, T.; Tétreault; Teuscher, J.; Gao, P.; Nazeeruddin, M. K.; Grätzel, M. *ACS Nano* **2014**, *8*, 362−373.
(27) Snaith, H. J.; Abate, A.; Ball, J. M.; Eperon, G. E.; Leijtens, T.; Noel, N. K.; Stranks, S. D.; Wang, J. T.-W.; Wojciechowski, K.; Zhang, W. *J. Phys. Chem. Lett.* **2014**, *5*, 1511−1515.
(28) Sanchez, R. S.; Gonzalez-Pedro, V.; Lee, J.-W.; Park, N.-G.; Kang, Y. S.; Mora-Sero, I.; Bisquert, J. *J. Phys. Chem. Lett.* **2014**, *5*, 2357−2363.
(29) Kim, H.-S.; Park, N.-G. *J. Phys. Chem. Lett.* **2014**, *5*, 2927−2934.
(30) Unger, E. L.; Hoke, E. T.; Bailie, C. D.; Nguyen, W. H.; Bowring, A. R.; Heumüller, T.; Christoforo, M. G.; McGehee, M. D. *Energy Environ. Sci.* **2014**, *7*, 3690−3698.
(31) Chen, H.-W.; Sakai, N.; Ikegami, M.; Miyasaka, T. *J. Phys. Chem. Lett.* **2015**, *6*, 164−169.
(32) Gottesman, R.; Haltzi, E.; Gouda, L.; Tirosh, S.; Bouhadana, Y.; Zaban, A.; Mosconi, E.; De Angelis, F. *J. Phys. Chem. Lett.* **2014**, *5*, 2662−2669.
(33) Tress, W.; Marinova, N.; Moehl, T.; Zakeeruddin, S. M.; Nazeeruddin, M. K.; Grätzel, M. *Energy Environ. Sci.* **2015**, *8*, 995−1004.
(34) Giannozzi, P.; Baroni, S.; Bonini, N.; Calandra, M.; Car, R.; Cavazzoni, C.; Ceresoli, D.; Chiarotti, G. L.; Cococcioni, M.; Dabo, I.; Dal Corso, A.; de Gironcoli, S.; Fabris, S.; Fratesi, G.; Gebauer, R.; Gerstmann, U.; Gougoussis, C.; Kokalj, A.; Lazzeri, M.; Martin-Samos, L.; Marzari, N.; Mauri, F.; Mazzarello, R.; Paolini, S.; Pasquarello, A.; Paulatto, L.; Sbraccia, C.; Scandolo, S.; Sclauzero, G.; Seitsonen, A. P.; Smogunov, A.; Umari, P.; Wentzcovitch, R. M. *J. Phys.: Condens. Matter* **2009**, *21*, 395502.
(35) Hamada, I. *Phys. Rev. B: Condens. Matter Mater. Phys.* **2014**, *89*, 121103(R).
(36) Kawamura, Y.; Mashiyama, H.; Hasebe, K. *J. Phys. Soc. Jpn.* **2002**, *71*, 1694−1697.
(37) Pang, S.; Hu, H.; Zhang, J.; Lv, S.; Yu, Y.; Wei, F.; Qin, T.; Xu, H.; Liu, Z.; Cui, G. *Chem. Mater.* **2014**, *26*, 1485−1491.
(38) Wang, Y.; Gould, T.; Dobson, J. F.; Zhang, H.; Yang, H.; Yao, X.; Zhao, H. *Phys. Chem. Chem. Phys.* **2014**, *16*, 1424−1429.
(39) Amat, A.; Mosconi, E.; Ronca, E.; Quarti, C.; Umari, P.; Nazeeruddin, M. K.; Grätzel, M.; De Angelis, F. *Nano Lett.* **2014**, *14*, 3608−3616.
(40) Pellet, N.; Teuscher, J.; Maier, J.; Grätzel, M. *Chem. Mater.* **2015**, *27*, 2181−2188.
(41) Colella, S.; Mosconi, E.; Fedeli, P.; Listorti, A.; Gazza, F.; Orlandi, F.; Ferro, P.; Besagni, T.; Rizzo, A.; Calestani, G.; Gigli, G.; De Angelis, F.; Mosca, R. *Chem. Mater.* **2013**, *25*, 4613−4618.
(42) Giorgi, G.; Fujisawa, J.-I.; Segawa, H.; Yamashita, K. *J. Phys. Chem. C* **2015**, *119*, 4694−4701.
(43) Goodenough, J. B. *Nature* **2000**, *404*, 821−823.
(44) Van der Ven, A.; Ceder, G.; Asta, M.; Tepesch, P. D. *Phys. Rev. B: Condens. Matter Mater. Phys.* **2001**, *64*, 184307.
(45) Tripathi, N.; Yanagida, M.; Shirai, Y.; Masuda, T.; Miyano, K. *J. Mater. Chem. A* **2015**, *3*, 12081.
(46) Nie, W.; Tsai, H.; Asadpour, R.; Blancon, J.-C.; Neukirch, A. J.; Gupta, G.; Crochet, J. J.; Chhowalla, M.; Tretiak, S.; Alam, M. A.; Wang, H.-L.; Mohite, A. D. *Science* **2015**, *347*, 522−525.
(47) Mei, A.; Li, X.; Liu, L.; Ku, Z.; Liu, T.; Rong, Y.; Xu, M.; Hu, M.; Chen, J.; Yang, Y.; Grätzel, M.; Han, H. *Science* **2014**, *345*, 295−298.

DOI: 10.1021/jacs.5b03615
J. Am. Chem. Soc. 2015, 137, 10048−10051